MS THESIS REPORT

Low Temperature Raman Study on Spinel Co_3O_4

PH5201

BY

TWISHUM TAH (20MS115)

BS-MS DUAL DEGREE MAY, 2025

SUPERVISED BY

DR. GOUTAM DEV MUKHERJEE

to

DEPARTMENT OF PHYSICS

IISER KOLKATA

CAMPUS ROAD, MOHANPUR, HARINGHATA FARM, WEST BENGAL, 741246

Endorsement and Verification

This is to certify that the work titled **'Low Temperature Raman Study on Spinel Co_3O_4'** submitted by **Twishum Tah** in partial fulfillment of the requirements for the degree of **BS-MS Integrated Dual Degree** at **IISER Kolkata** is an authentic record of research carried out under my supervision.

Signature of the Candidate:

Twishum Tah

Name: Twishum Tah

Signature of the Supervisor:

Goutam Mukherjee 02/06/2022

Name: Dr. Goutam Dev Mukherjee
Designation: Professor
Department: Department of Physical Sciences
Institution: IISER Kolkata

Contents

1 Abstract

This thesis provides an extensive investigation into the structural and vibrational properties of cobalt oxide (Co_3O_4) by employing detailed low-temperature Raman spectroscopy, offering an in-depth examination of potential phase transitions at cryogenic conditions.

Co_3O_4, a spinel oxide with considerable interest in fields such as energy storage, catalysis, sensors, and electronic devices, has traditionally been examined predominantly under ambient conditions. However, its detailed low-temperature properties remain insufficiently characterized, leading to a significant gap in condensed matter physics literature and limiting the exploitation of its full technological potential.

In this comprehensive study, we have synthesized highly crystalline Co_3O_4 samples via solid-state reaction methods optimized to ensure reproducibility and purity.

The samples underwent rigorous characterization through advanced techniques, including X-ray diffraction (XRD), scanning electron microscopy (SEM), and energy-dispersive X-ray spectroscopy (EDX), validating both their crystal structure and chemical homogeneity.

Subsequent to characterization, an extensive low-temperature Raman spectroscopy campaign was executed, covering temperatures systematically from ambient conditions down to near-liquid helium temperatures.

This experimental setup enabled precise detection and monitoring of subtle spectral variations, frequency shifts, and alterations in phonon linewidths, which are sensitive indicators of structural changes, electronic alterations, or lattice dynamics modifications at reduced temperatures.

Significantly, our experimental observations reveal distinct anomalies within specific Raman-active phonon modes, including pronounced frequency shifts, mode splitting, and variations in relative intensities, clearly indicative of previously undocumented low-temperature structural or electronic phase transitions.

These findings are analyzed comprehensively within the framework of lattice distortion phenomena, electron-phonon coupling effects, and symmetry-breaking processes, further corroborated by comparison with relevant theoretical models from condensed matter physics.

This robust analytical approach not only bridges the existing gap in knowledge concerning Co_3O_4 at low temperatures but also sheds critical insight into its complex electronic and vibrational behaviors, thereby potentially influencing future technological implementations.

In conclusion, this research significantly advances the foundational understanding of low-temperature phase behaviors in Co_3O_4, providing crucial insights for the development of enhanced functional devices requiring precise performance at low temperatures.

Furthermore, the results presented herein lay solid groundwork for future studies, opening pathways to novel applications and deeper explorations within the broader landscape of spinel oxides and related materials.

2 Acknowledgements

I would like to express my deepest gratitude to my advisor, Professor Goutam Dev Mukherjee, for his invaluable guidance, continuous support, and encouragement throughout my research. His insightful suggestions and dedicated mentorship were instrumental in the successful completion of this thesis.

I am also profoundly grateful to my lab seniors, Asish Kumar Mishra, Bhagyashree Giri, and Bidisha Mukherjee, for their immense support, fruitful discussions, critical insights, and continuous assistance throughout the course of my experimental work.

Finally, I extend my heartfelt appreciation to my family and friends (both real and digital) for their constant emotional support and encouragement during this academic journey.

3 Introduction

In recent years, transition metal oxides, particularly spinel oxides, have attracted considerable attention from researchers across disciplines due to their exceptional physical, electronic, and catalytic properties. Among these, cobalt oxide (Co_3O_4), with its unique spinel crystal structure, stands out prominently. The intrinsic versatility of Co_3O_4 manifests in its ap-

plicability across various advanced technological domains, including energy storage systems, electrochemical sensors, heterogeneous catalysis, magnetic materials, and electronic devices. However, while extensive research efforts have significantly clarified its properties at room temperature, a critical knowledge gap persists concerning its low-temperature behavior, particularly its structural stability, vibrational dynamics, and potential phase transitions.

The study of materials at low temperatures provides a window into their fundamental physical properties, uncovering phenomena otherwise obscured by thermal fluctuations at higher temperatures. This is especially relevant in materials exhibiting rich electronic, magnetic, or structural phenomena governed by subtle interactions, such as electron-phonon coupling, spin-lattice interactions, and symmetry-breaking transitions. Raman spectroscopy, as a non-destructive optical characterization method, is exceptionally sensitive to structural changes, vibrational mode dynamics, and phase transitions at the atomic scale, making it an ideal analytical tool for exploring these low-temperature phenomena.

Cobalt oxide (Co_3O_4), belonging to the spinel oxide family, crystallizes in the normal spinel structure characterized by cobalt ions distributed among octahedral and tetrahedral sites. The interplay between these structural components and electronic states imparts complex physical properties that significantly depend on temperature variations. Prior investigations have primarily documented the room-temperature properties of Co_3O_4, describing its standard cubic spinel structure, magnetic ordering, and catalytic behavior extensively. However, comprehensive low-temperature explorations remain limited, leaving its full scientific and technological potential underexplored.

Motivated by this gap, this thesis systematically investigates the structural and vibrational properties of Co_3O_4 at low temperatures through Raman spectroscopy, aiming to elucidate potential phase transitions and associated structural or electronic anomalies. To accomplish this, high-quality crystalline Co_3O_4 samples were synthesized using optimized solid-state reaction techniques, rigorously characterized via complementary analytical methods such as X-ray diffraction (XRD), scanning electron microscopy (SEM), and energy-dispersive X-ray spectroscopy (EDX) to confirm structural integrity and compositional purity.

Subsequently, extensive Raman spectroscopy measurements were performed systematically over a wide temperature range, from ambient conditions down to cryogenic temperatures approaching liquid helium environments. This meticulous approach permitted the careful de-

tection and documentation of subtle yet significant spectral alterations, such as phonon mode shifts, splitting, and intensity changes, directly associated with low-temperature phase transitions and structural modifications. Detailed analysis of these findings, supported by theoretical modeling rooted in fundamental condensed matter physics principles, provides unprecedented insights into the vibrational behavior, structural dynamics, and electron-phonon interactions of Co_3O_4 at low temperatures.

The primary objective of this thesis is thus to fill the critical knowledge gap in the literature regarding low-temperature phase transitions and associated physical phenomena in Co_3O_4. By systematically examining these previously unexplored temperature-dependent behaviors, this work not only advances the fundamental understanding of spinel oxide materials but also significantly impacts the potential future development of technologically advanced devices requiring stability and consistent performance at reduced temperatures.

4 Theory of Condensed Matter and Spectroscopy:

4.1 Basics of Condensed Matter Physics

Condensed matter physics investigates the macroscopic and microscopic physical properties of matter, particularly focusing on solids and liquids. At its core, condensed matter physics explores phenomena arising from interactions between a large number of atoms or molecules. These collective interactions lead to complex behaviors not exhibited by individual atoms alone, such as superconductivity, magnetism, and structural phase transitions. Understanding these phenomena is crucial both fundamentally and for advancing numerous technological applications.

Solids are primarily categorized as crystalline or amorphous, depending on the degree of atomic order. Crystalline solids, such as cobalt oxide (Co_3O_4), exhibit long-range order, characterized by periodic arrangement of atoms in a crystal lattice. The symmetry and periodicity of these lattices play a crucial role in determining the physical properties of solids, including their mechanical strength, thermal conductivity, electronic behavior, and vibrational characteristics.

One fundamental concept in condensed matter physics is the notion of phonons, which are

quantized vibrational modes arising from the collective oscillations of atoms within a crystal lattice. These phonons significantly impact various macroscopic properties such as heat capacity, thermal conductivity, and electron transport. Temperature-dependent studies, especially at low temperatures, are particularly informative because thermal energy variations can lead to subtle but critical structural and electronic transformations, identifiable via shifts or splitting of phonon frequencies.

Spinel oxides, such as Co_3O_4, crystallize in structures exhibiting distinct symmetry elements. Co_3O_4 specifically adopts a cubic spinel structure, characterized by Co ions in two different valence states occupying distinct lattice positions, which significantly affects its electronic and magnetic behavior. Detailed characterization of how temperature influences the lattice and electronic configurations of spinel oxides deepens our fundamental understanding of solid-state physics.

4.1.1 Phase Transitions in Solids:

A key phenomenon studied in condensed matter physics is phase transitions—transformations in the state or structure of matter as external parameters, like temperature or pressure, change.

Examples:

- **Structural:**Crystal symmetry changes (e.g. cubic → tetragonal)
- **Magnetic:** Paramagnetic (random spins) → Antiferromagnetic (ordered spins)
- **Electronic:** Insulator → Metal transition

At low temperatures, **low temperatures**, **reduced thermal energy** often allows **ordered states** (e.g. magnetic ordering) to emerge.

4.2 d-orbital Splitting - Foundation of Crytal Field Theory(CFT)

5 d-orbitals $d_{xy}, d_{yz}, d_{zx}, d_{x^2-y^2}, d_{z^2}$ do **not** remain **degenerate(equal in energy)** when **surrounded by ligands**. This phenomenon is known as **d-orbital splitting** and is central to **Crystal Field Theory(CFT)**.

4.2.1 Origin of d-orbital Splitting

When a transition metal ion is surrounded by ligands, the **negative charge of the ligands**, repels the **d-electrons** of the metal. However, not all d-orbitals experience the same amount of repulsion. The way they split depends on the **geometry of the ligand arrangement** around the metal.

4.2.2 d-orbital Splitting in Different Geometries

The most common geometries in coordination chemistry are **octahedral, tetrahedral and square-planar**

Octahedral Field Splitting:

1. In an **octahedral** complex, **6** ligands surround the metal in a symmetric arrangement.

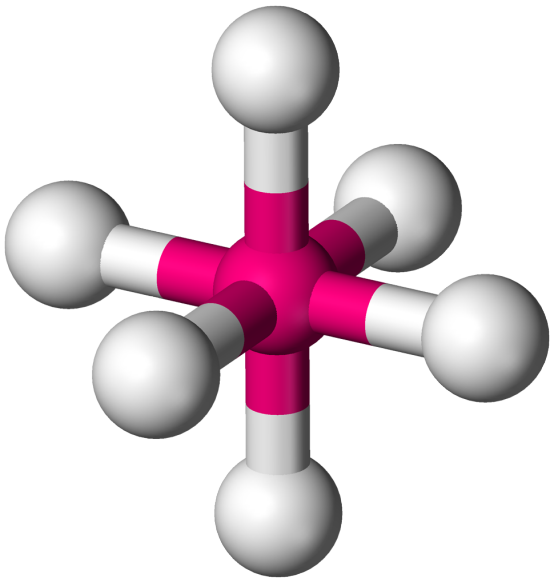

Figure 1: Octahedral 3D model

2. The d-orbitals split into two sets -

   - e_g (higher energy) $\rightarrow d_{x^2-y^2}, d_{z^2}$

     These orbitals point **directly at** the ligands $\rightarrow$ experience **more repulsion** $\rightarrow$ **higher energy**

   - t_{2g} (lower energy) $\rightarrow d_{xy}, d_{yz}, d_{zx}$

     These orbitals point **between** the ligands $\rightarrow$ experience **less repulsion** $\rightarrow$ **lower**

energy

3. The **energy difference** between the 2 sets is called **Crystal Field Splitting Energy** (**Δ_o** or **10 Dq**)

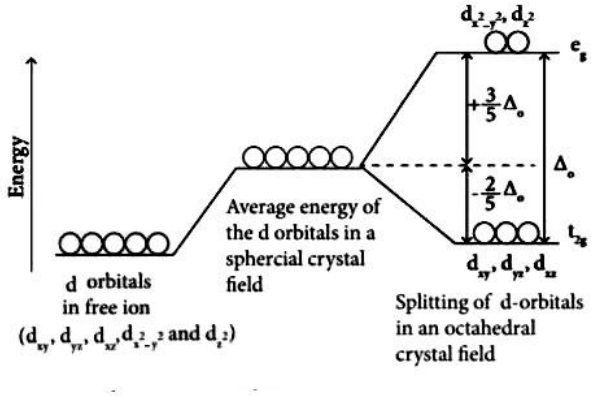

Figure 2: d-orbital splitting in octahedral complex

Electron Filling in Octahedral Fields

- **Weak field ligands** (small Δ_0) $\rightarrow$ **High-spin configuration** (electrons **spread out**)
- **Strong field ligands** (large Δ_0) $\rightarrow$ **low-spin configuration** (electrons **pair up in lower orbitals**)

Tetrahedral Field Splitting:

1. In an **tetrahedral** complex, **4** ligands surround the metal in a symmetric arrangement.
2. The d-orbitals split into two sets -
   - e_g (lower energy) $\rightarrow d_{x^2-y^2}, d_{z^2}$
     These orbitals point **between** the ligands $\rightarrow$ experience **less repulsion** $\rightarrow$ **lower energy**
   - t_{2g} (higher energy) $\rightarrow d_{xy}, d_{yz}, d_{zx}$
     These orbitals point **directly at** the ligands $\rightarrow$ experience **more repulsion** $\rightarrow$ **higher energy**
3. The **energy difference** between the 2 sets is called **Crystal Field Splitting Energy** (**Δ_t** ($\Delta_O \approx 4\Delta_t$)

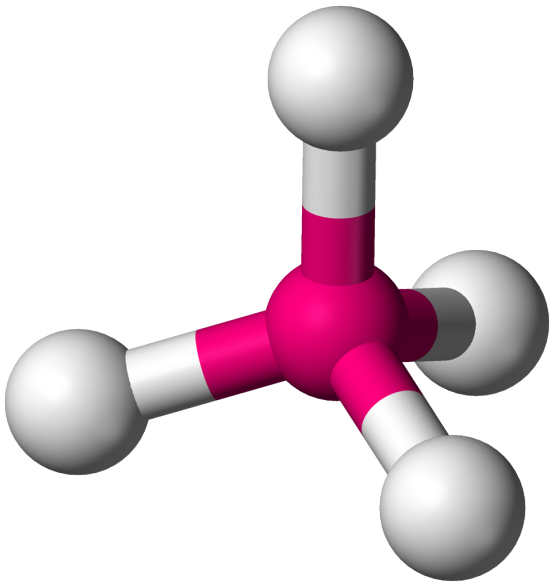

Figure 3: Tetrahedral 3D Model

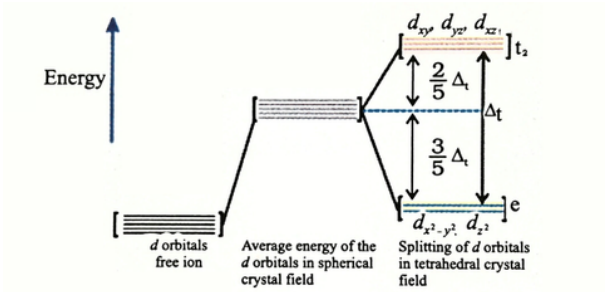

Fig.9.9: *d orbital splitting in a tetrahedral crystal field.*

Figure 4: d-orbital splitting in tetrahedral complex

Electron Filling in Tetrahedral Fields

- **Almost all** tetrahedral complexes are **high-spin** due to **small splitting**.

Square Planar Field Splitting

- A **square planar** geometry is **derived** from **octahedral** - but with 2 ligands removed.
- Splitting pattern becomes more **complex**.

4.2.3 Effect of d-orbital Splitting on Electrons:

1. **Color of complexes:**
    - **Energy gap** Δ determines the **wavelength of light absorbed**

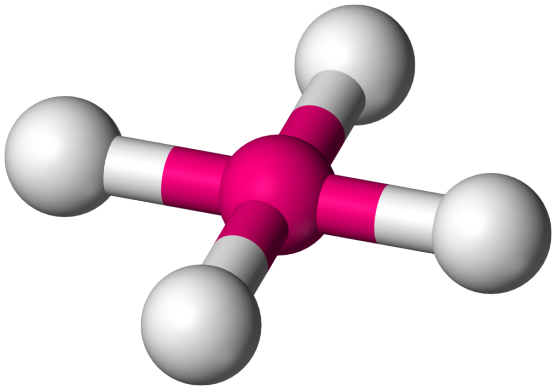

Figure 5: Square Planar 3D Model

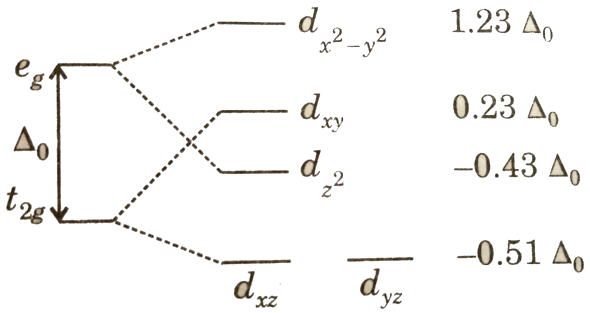

Figure 6: Square-planar splitting

- Complexes appear **colored** because they absorb specific wavelengths and **transmit** others.
- **Larger splitting** (Δ_o) $\rightarrow$ Absorb **higher energy light(blue or violet** $\rightarrow$ Appear **yellow or red**
- **Smaller splitting** (Δ_o) $\rightarrow$ Absorb **lower energy light(yellow or red** $\rightarrow$ Appear **blue or green**

2. **Magnetism:**
   - **High-spin complexes** $\rightarrow$ **Unpaired** electrons $\rightarrow$ **Paramagnetic**
   - **Low-spin complexes** $\rightarrow$ All electrons **paired** $\rightarrow$ **Diamagnetic**
3. **Stability and Reactivity**
   - **Large Δ strong field ligands** $\rightarrow$ More **stable low-spin state**
   - **Small Δ weak field ligands, like oxo ligands** $\rightarrow$ More **stable high-spin state**

4.2.4 Can Stability Change?

Stability of **high spin versus low spin states can change due to**:

- **Temperature** → Some materials undergo **spin transitions** at **low or high temperatures**
- **Pressure** → High pressure can force electrons to pair, leading to a **high spin to low spin transition**
- **Ligand exchange** → Changing ligands alters $\boldsymbol{\Delta_o}$, shifting the balance between high spin and low spin states.

4.3 Raman Spectroscopy

Raman spectroscopy is a powerful and non-destructive optical characterization technique widely employed to study vibrational, rotational, and other low-frequency modes in a material. It involves illuminating a sample with monochromatic light (typically from a laser), detecting scattered photons that emerge with frequency shifts due to interactions with vibrational states. This scattering effect, known as Raman scattering, occurs due to the inelastic interaction between incident photons and phonons or other excitations within the material.
The frequency shifts (Raman shifts) observed in Raman spectroscopy are directly related to specific vibrational modes, providing detailed information on the material's molecular and crystal structure. Raman spectroscopy is highly sensitive to small changes in lattice dynamics, symmetry, and electronic configurations, making it exceptionally suitable for investigating subtle structural transitions, lattice distortions, and electron-phonon interactions, especially at low temperatures where such subtle changes become pronounced.

4.4 Raman Spectroscopy and Condensed Matter Physics

In condensed matter physics, Raman spectroscopy serves as a non-destructive probe to study vibrational dynamics and lattice behavior under varying conditions. Low-temperature Raman studies are particularly valuable, as decreasing temperature can enhance spectral resolution and highlight subtle structural or electronic transitions masked at higher temperatures. Phenomena like phonon softening, mode splitting, and changes in phonon linewidth are sensitively detected by Raman spectroscopy, thus providing clear evidence of phase transitions or lattice distortions.

In the context of Co_3O_4, Raman spectroscopy is especially informative. The compound's distinct vibrational modes, originating from interactions between oxygen and cobalt ions in their spinel lattice sites, are highly responsive to structural changes induced by temperature variations. By carefully tracking changes in these modes, low-temperature Raman spectroscopy can provide critical insights into the material's lattice stability, electronic transitions, and structural integrity.

Furthermore, understanding the observed spectral changes demands complementary theoretical insights, typically provided by group theory and density functional theory (DFT) calculations. Group theory helps classify the allowed Raman-active vibrational modes based on the symmetry of the crystal structure, while DFT simulations provide quantitative predictions of the vibrational frequencies, electronic structures, and their dependence on temperature. This combined experimental-theoretical approach allows for a robust interpretation of Raman data, connecting experimental observations to fundamental lattice dynamics and electronic structure.

Overall, the synergy between Raman spectroscopy, condensed matter theoretical frameworks, and complementary characterization techniques represents an essential methodological foundation, enabling detailed exploration of Co_3O_4's complex low-temperature behaviors. This theoretical and methodological integration forms the cornerstone upon which the findings and analyses of this thesis rest.

4.5 Stokes and Anti-Stokes scattering

At temperature T, the population of phonons follow the **Bose Einstein distribution**:

$$\boxed{n(\omega, T) = \frac{1}{e^{\frac{\hbar\omega}{k_B T}} - 1}},$$

where,

- $\hbar \rightarrow$ reduced Planck's constant
- $\omega \rightarrow$ Phonon frequency
- $k_B \rightarrow$ Boltzmann constant
- $T \rightarrow$ absolute temperature

At low temperature ($k_B T \ll \hbar\omega$),

$$\boxed{n(\omega, T) \approx e^{\frac{\hbar\omega}{k_B T}}}$$

Therefore, **at low temperature anti-Stokes scattering (where phonon is annihilated) becomes rare and Stokes' scattering (where phonon is created) dominates.**

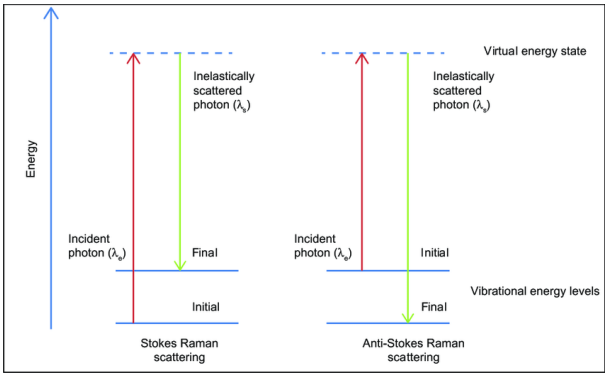

Figure 7: Stokes' and Anti-stokes' Raman

4.6 Stokes Scattering: Phonon creation

$$\boxed{|i\rangle = |0\rangle_{\text{phonon}} + |\hbar\omega_L\rangle_{\text{photon}}}$$

$$\boxed{|i\rangle = |1\rangle_{\text{phonon}} + |\hbar\omega_S\rangle_{\text{photon}}}$$

where,

- $|0\rangle$ represent the phonon occupation number before scattering
- $|1\rangle$ represent the phonon occupation number after scattering
- $|\hbar\omega_L\rangle_{\text{photon}}$ represent the initial photon state
- $|\hbar\omega_S\rangle_{\text{photon}}$ represent the final photon state

4.6.1 Quantum Mechanical Interpretation

Mathematically, this corresponds to the **creation of a phonon**, described by the phonon creation operator $a^+_{\vec{q},\lambda}$:

$$\boxed{H_{\text{int}} |0\rangle_{\text{phonon}} = C a^{+}_{\vec{q},\lambda} |0\rangle_{\text{phonon}}}$$

where,

C is a coefficient dependent on light matter interaction.

4.6.2 Experimental Signature

- Raman spectra exhibits a **Stokes' peak** at $(\boldsymbol{\omega_L - \omega_{\vec{q},\lambda}})$
- Intensity of the Stokes' peak **does not depend on temperature** since phonons can always be created regardless of the initial phonon population

4.7 Anti-Stokes Scattering: Phonon Annihilation

$$\boxed{|i\rangle = |1\rangle_{\text{phonon}} + |\hbar\omega_L\rangle_{\text{photon}}}$$

$$\boxed{|f\rangle = |0\rangle_{\text{phonon}} + |\hbar\omega_{\text{aS}}\rangle_{\text{photon}}}$$

where:

- $|1\rangle$ represent the phonon occupation number before scattering
- $|0\rangle$ represent the phonon occupation number after scattering
- $|\hbar\omega_L\rangle_{\text{photon}}$ represent the initial photon state
- $|\hbar\omega_{\text{aS}}\rangle_{\text{photon}}$ represent the final photon state

4.7.1 Quantum Mechanical Interpretation

Mathematically, this corresponds to the **annihilation of a phonon**, described by the phonon annihilation operator $a_{\vec{q},\lambda}$:

$$\boxed{H_{\text{int}} \left|1\right\rangle_{\text{phonon}} = C a_{\vec{q},\lambda} \left|1\right\rangle_{\text{phonon}}}$$

where,

C is a coefficient dependent on **light matter interaction.**

4.7.2 Experimental Signature

- Raman spectra exhibits a **Anti-Stokes' peak** at **(**$\omega_L + \omega_{\vec{q},\lambda}$
- Intensity of the Anti-Stokes' peak **is strongly temperature-dependent** since phonon annihilation requires the presence of a thermally excited phonon

4.8 Raman Scattering Cross-section

Differential Raman scattering cross-section is given by

$$\boxed{\frac{d\sigma}{d\Omega d\omega} \propto S(\vec{q}, \omega)}$$

where,

- $d\sigma \rightarrow$ infinitesimal scattering intensity (scattering probability)
- $d\Omega \rightarrow$ solid angle element in which scattered photons are collected
- $d\omega \rightarrow$ frequency (or energy) range of the photons
- $S(\vec{q}, \omega) \rightarrow$ Dynamical structure factor

This equation **characterizes how phonons (or other excitations) contribute to scattering.**

4.8.1 $d\Omega$

$d\Omega$ is the solid angle element in which scattered photons are collected and is defined as follows:

$$\boxed{d\Omega = \sin\theta d\theta d\phi}$$

where:

- $\theta \rightarrow$ azimuthal angle in the xy-plane
- $\phi \rightarrow$ polar angle from the z-axis

4.8.2 Dynamical Structure Factor

The dynamical structure factor ($S(\vec{q}, \omega)$) describes the probability of creating or annihilating a phonon of **momentum q and energy $\hbar\omega$**

4.9 Momentum Conservation in Raman scattering

$$\boxed{\vec{q} = \vec{k_{incident}} - \vec{k_{scattered}}}$$

where

$\vec{k} \rightarrow wavevector$

Since photons have very small momenta compared to phonons in a crystal, **Raman scattering typically probes only phonons near** $\vec{q} \approx 0$(zone-centre phonons)

4.10 Light-Phonon coupling

Interaction of light with crystal lattice can be understood in terms of the electric polarizability tensor ($\vec{R}$), which depends on the atomic displacements caused by phonons. In quantum mechanical terms, a phonon is an elementary excitation of the lattice vibrations, described by bosonic creation and annihilation operators:

- Phonon creation operator: $a^{+}_{\vec{q},\lambda}$ (adds a phonon of wavevector $\vec{q}$ and mode λ
- Phonon annihilation creator: $a_{\vec{q},\lambda}$ (removes a phonon)

The interaction Hamiltonian for the light-phonon coupling can be written as:

$$\boxed{H_{int} \propto (\vec{e} \cdot \vec{R} \cdot \vec{e'})(a_{\vec{q},\lambda} + a^{+}_{\vec{q},\lambda})}$$

where,

- $\vec{e} \rightarrow$ polarisation vector of incident photons
- $\vec{e'} \rightarrow$ polarisation vector of scattered photons

4.11 Role of phonon lifetime and linewidth

The **Raman linewidth (Γ)** is related to the **phonon lifetime (τ)** by the uncertainty principle:

$$\boxed{\Gamma \approx \frac{1}{\tau}}$$

At low temperatures, phonon decay channels (like phonon-phonon scattering) become suppressed, leading to **longer phonon lifetimes** and **narrower Raman peaks**.

4.12 Phonon Density of States and Selection Rules

Raman response function can be expressed using the **phonon density of states (DOS)**:

$$\boxed{S(\omega) \propto \sum_{(\vec{q},\lambda)} \underbrace{|\vec{e} \cdot \vec{R} \cdot \vec{e'}|^2}_{\text{scattering probability}} \quad \delta(\omega - \omega_{\vec{q},\lambda})}$$

where,

- $S(\omega) \rightarrow$ Raman Scattering Intensity at frequency ω
- $\vec{e} \rightarrow$ polarisation vector of incident light
- $\vec{e'} \rightarrow$ polarisation vector of scattered light
- $\vec{R} \rightarrow$ Raman Tensor or Polarizability Tensor
- $\omega_{\vec{q},\lambda} \rightarrow$ phonon frequency for mode λ at wave-vector q

S(ω) describes how light interacts with phonons, leading to shifts in the scattered light frequency.

$\delta(\omega - \omega_{\vec{q},\lambda})$ ensures that only phonon modes with frequency $\omega_{\vec{q},\lambda}$ contributes to the scattering at the observed Raman shift ω. This forces **energy conservation**, the frequency of the scattered photon is shifted by an amount corresponding to the phonon frequency.

5 Practical Aspects

5.1 FWHM (ω)-Why does a Peak have a width?

At the most fundamental level, the width of a Raman peak is dictated by **quantum uncertainty** and **decoherence**

5.1.1 Why do Raman peaks have width?

- In an **ideal, isolated quantum system**, energy levels are **sharp and discrete**, meaning the Raman peaks would be definitely narrow.
- In reality, **energy levels are not perfectly sharp** because:

1. **Finite lifetime (Energy-Time Uncertainty principle)**

   The lifetime of a phonon mode (τ) is finite because phonons are not perfectly stable - they decay due to interactions with other phonons, electrons or lattice defects.

   The **energy uncertainty principle** gives:

$$\boxed{\Delta E.\Delta t \geq \frac{\hbar}{2}}$$

   Since $\boldsymbol{\Delta E}$ **is related to FWHM and** $\boldsymbol{\Delta t}$ **is phonon lifetime**, we see that a shorter lifetime leads to broader peaks.

2. **Decoherence and Many Body Interactions**

   Phonons in a real material are constantly interacting with each other. These interactions cause **random phase shifts**, leading to **spectral broadening.** The more interactions (e.g. phonon-phonon scattering at high temperatures), the broader the peak.

5.1.2 Why does FWHM increase with temperature?

At higher temperatures:

- More **phonon-phonon scattering** occurs (due to increased occupation of phonon states from the **Bose-Einstein** distribution)

- More **anharmonicity** in the atomic potential (the restoring force is purely quadratic)
- More **defect scattering** due to thermal expansion and disorder.

All these effects **shorten phonon lifetime, increasing FWHM**.

Fundamental Answer The Raman peak width arises because **quantum states are not perfectly isolated**- they interact with their environment, and the phonons' finite lifetime results in a broadened energy spectrum. This effect increases with temperature because **thermal fluctuations enhance quantum decoherence and anharmonic interactions.**

5.2 Peak frequency (x_c) - Why does a vibrational frequency shift?

The Raman shift (x_c) corresponds to the **energy of a vibrational mode**, which is **directly determined by the restoring force of atomic bonds.**

Why do phonon frequencies shift with temperature? The fundamental equation governing atomic vibrations in a solid is:

$$\boxed{\omega = \sqrt{\frac{k}{m}}}$$

where,

- $\omega \rightarrow$ **vibrational frequency**
- k $\rightarrow$ **effective spring constant** of the atomic bond
- m $\rightarrow$ **atomic mass**

At higher temperatures:

1. **Lattice expansion (Bond softening):**
    - The potential energy of atomic bonds is **not perfectly harmonic** (the real atomic potential has an assymetric shape)
    - As temperature increases, atoms vibrate with **larger amplitudes** shifting into regions of the potential where the curvature (k) is lower.

- This **reduces the restoring force**, leading to **a decrease in vibrational frequency (phonon softening)**.

2. **Anharmonic effects (Self Energy Corrections)**

   - The real phonon energy is modified due to **higher order interactions** (phonon-phonon interactions shift the energy levels)
   - This can cause the frequency to shift in either direction, depending on the material and the specific interaction.

5.2.1 Why does the centre of gravity of the peak give the vibrational frequency?

- The centre of gravity of a peak:

$$\boxed{x_c = \frac{\int xI(x)dx}{\int I(x)dx}}$$

  , provides the **average energy** of all phonon states contributes to the Raman scattering

- If the peak is **asymmetric** (due to multiple phonon contributions or Fano interference), the **true phonon frequency** is not just the peak maximum but the **weighted mean** of the spectral distribution.
- The centre of gravity ensures we account for all energy states contributing to the mode.

Fundamental answer

Phonon frequencies shift with temperature because **the atomic bonding force weakens due to lattice expansion and anharmonic interactions**. The centre of gravity is used because it represents the **true average phonon energy**, unaffected by peak asymmetry.

5.3 Area Integral (Intensity)- Why does Raman Intensity change?

The total integral of a Raman peak represents the **total scattered photon count:**

$$\boxed{I_{\text{total}} = \int I(x)dx}$$

which is governed by :

1. The number of phonons available for scattering (phonon population)
2. The probability of Raman scattering occuring (cross-section)

5.3.1 Why does phonon population change with temperature?

- Phonon states follow **Bose-Einstein statistics:**

$$\boxed{n(T) = \frac{1}{e^{\frac{h\nu}{k_B T}} - 1}}$$

- As **temperature increases**, n(T) increases, meaning **more phonons exist to participate in scattering**, which should increase intensity.
- However, Raman intensity depends only on phonon population but also on **how efficiently light interacts with these phonons**

5.3.2 Why does Intensity sometimes decrease with temperature?

1. **Broadening effects reduce peak height**
   - Even though more phonons exist, the **broadening of the peak spreads intensity over a large range**, reducing the peak height while keeping the total area nearly constant.
2. **Increased Anharmonicity weakens Raman Scattering efficiency**
   - At very high temperatures, **disorder and anharmonicity** reduce the probability of a coherent Raman scattering event.
   - This can **suppress intensity,** despite higher phonon numbers.
3. **Phase Transitions change Raman selection rules**
   - If a material undergoes a **phase transition**, the Raman active modes may **disappear** (due to symmetry changes), leading to a sudden drop in intensity.

5.3.3 Why does the area integral give the total phonon intensity?

- The **peak height alone is not a reliable measure**, because it is affected by peak broadening.
- The **total area under the peak** represents the **integrated phonon population participating in Raman scattering**
- This makes it a **better metric for studying temperature dependent phonon behavior.**

Fundamental Answer

The Intensity (area integral) represents the **total Raman-scattered count**, which is governed by phonon population and scattering probability. It changes with temperature because **phonon occupation increases, but broadening and anharmonicity affect how effectively light interacts with them**.

5.4 Why do we study these trends?

1. **FWHM** tells us about **phonon lifetime** and **quantum decoherence**.
2. **Peak position (x_c)** tells us about **bond strength and lattice dynamics.**
3. **Intensity(integral)** tells us about **phonon population and scattering probability**. At the deepest level, these trends arise because **real physical systems are not isolated** - they interact with their environment and temperature changes **modify the quantum states of phonons**, leading to observable shifts in their behavior.

6 Co_3O_4 Basic Structure and Properties

6.1 Chemical Basics of Co_3O_4

- Formula $\rightarrow$ Co_3O_4 (Cobalt (II,III) oxide)
- Composition $\rightarrow$ Made of Co and O atoms

6.2 Composition and Structure:

Co_3O_4 is a cobalt oxide with a spinel structure (general formula AB_2O_4). It contains -

- Co^{2+} ions in tetrahedral sites (4 oxygen neighbours)
- Co^{3+} ions in octahedral sites (6 oxygen atoms)
- The structure is cubic (space group Fd-3m) at room temperature

6.3 Magnetic properties

$\boldsymbol{Co^{2+}}$ is **magnetic (high spin state)**, while $\boldsymbol{Co^{3+}}$ is **non-magnetic (low spin)**. This leads to **antiferromagnetic ordering** below $\sim \boldsymbol{40K}$ (Néel temperature), where spins align oppositely.

6.4 Co_3O_4's Known Low Temperature Behavior

- **Magnetic Transition:** Below $\sim \boldsymbol{40K}$, Co_3O_4 becomes **anti-ferromagnetic** due to $\boldsymbol{Co^{2+}}$ **ordering**.
- **Structural Stability:** The **cubic** spinel **structure** is generally **stable**, but subtle distortions (e.g. **bond length changes** may occur at low temperatures.

Co_3O_4 is a **normal spinel**. Even in the presence of weak field oxo ligands Co^{3+} is a **low spin** d^6 **ion** with **very high CFSE on the octahedral sites**, because of the **high charge** and **small size** of the Co^{3+} ion.

Hence the Co^{3+} ions occupy **both octahedral sites** and Co^{2+} occupies the tetrahedral site.

6.5 Spin States of Co Ions in Co_3O_4

Co_3O_4 has **both** high-spin and low-spin cobalt ions:

- Co^{2+} (d^7, tetrahedral) $\rightarrow$ High spin
- Co^{3+} (d^6, octahedral) $\rightarrow$ Low spin

6.5.1 Why does Co^{3+} become low spin?

- Co^{3+} has **higher oxidation state**, which increases **ligand field splitting** ($\boldsymbol{\Delta_o}$)
- The **octahedral $\boldsymbol{Co^{3+}}$ sites** experience **strong enough splitting** to favor **low spin**.

6.5.2 Why does Co^{2+} remain high spin?

- Co^{2+} has a **lower oxidation state**, meaning the **ligand field** is **not strong enough** to force **pairing**.
- It is **tetrahedral**, where $\boldsymbol{\Delta_t}$ **is too small to induce a low-spin state**.

6.5.3 Is Co_3O_4 stable?

Combination of low-spin $\boldsymbol{Co^{3+}}$ and high spin $\boldsymbol{Co^{2+}}$ is **extremely stable**. This **mixed valence state** stabilizes the crystal structure , making Co_3O_4 a **highly stable, inert** material.

6.6 Magnetic Properties of Co_3O_4

Co_3O_4 exhibits intriguing magnetic properties that vary with temperature, particularly transitioning from **paramagnetic** behavior at **room temperature** to **antiferromagnetic ordering** at **low temperatures.**

6.6.1 Room Temperature Behavior:

Paramagnetism:

At ambient conditions, Co_3O_4 behaves like a paramagnetic material, meaning it does **not** exhibit **spontaneous magnetisation** but can be **weakly magnetised** in the **presence** of an **external magnetic field**.

- At **room temperature**, Co_3O_4 behaves like a **paramagnet** because **thermal energy disrupts** any **magnetic ordering** keeping the spins **randomly oriented**.
- Co^{2+} and Co^{3+} ions in Co_3O_4 contribute to its **weak paramagnetic response**.
- As the **temperature decreases**, the **random thermal motion reduces** and Co_3O_4 undergoes a transition to an **ordered state (antiferromagnetic)**.

6.6.2 Low Temperature Behavior:

Antiferromagnetic Transition: As the **temperature decreases**, Co_3O_4 undergoes a **transition** to an **antiferromagnetic state** at its **Néel temperature** ($\boldsymbol{T_N}$) This temperature is reported to be around **30 K** in some studies, while others it at approximately **40K**. In this **antiferromagnetic state**, the **magnetic moments** of $\boldsymbol{Co^{2+}}$ ions align in an **anti-parallel configuration**, resulting in **no net macroscopic magnetisation**.

- As temperature **decreases below** the Néel temperature ($\boldsymbol{T_N \approx 30 - 40K}$, Co_3O_4 transitions from **paramagnetic to antiferromagnetic order**
- Co^{2+} and Co^{3+} ions form an **anti-parallel spin arrangement**, leading to **zero net magnetisation**.
- Co_3O_4 does **not** become a permanent magnet cause its spins cancel each other out.

7 Literature Review

7.1 Introduction

Cobalt oxide (Co_3O_4) has gained significant attention in the condensed matter community due to its unique crystal structure and remarkable physical properties. The interest is largely driven by potential technological applications such as energy storage, catalysis, sensors, and magnetic materials. While numerous studies explore Co_3O_4 at room temperature, systematic research into its low-temperature vibrational properties and phase transitions remains limited.

7.2 Raman Spectroscopy of Co_3O_4: Fundamental Studies

A foundational study by Hadjiev et al. (1988) investigated the Raman-active phonon modes of single-crystal Co_3O_4. They accurately characterized five distinct Raman modes at room temperature—194, 482, 522, 618, and $691 cm^{-1}$ —attributed to vibrational symmetries within its spinel crystal structure. Hadjiev and colleagues assigned these peaks precisely using factor group analysis, providing essential reference data for future comparative studies. Furthermore, they identified a clear temperature dependence of these vibrational modes, particularly noting a pronounced shift in the $691 cm^{-1}$ peak with temperature, quantified as approximately $3.9 \times$

$10^{-2}cm^{-1}/K$. This work laid critical groundwork for subsequent temperature-dependent Raman investigations of Co_3O_4

7.3 Structural Modifications and Raman Response

Furthering understanding of Co_3O_4's structural sensitivity, Wang et al. (2019) systematically examined structural modifications through formic acid treatment. Their results demonstrated that even subtle structural alterations significantly impact Raman spectra. Formic acid treatment notably reduced crystallite size and increased surface defects, leading to distinct shifts and broadening of Raman peaks. These shifts were attributed to phonon confinement effects, resulting directly from the reduced particle sizes and increased surface irregularities. Crucially, this demonstrated Raman spectroscopy's sensitivity to structural changes in Co_3O_4, thereby validating it as an effective probe for examining subtle lattice modifications and surface phenomena.

7.4 Low-Temperature Phase Transitions in Related Spinel Oxides

While direct low-temperature studies of Co_3O_4 remain sparse, several related spinel oxides exhibit significant phase transitions at reduced temperatures. For instance, magnetite (Fe_3O_4) undergoes the well-known Verwey transition at approximately 120 K, characterized by pronounced Raman spectral changes due to charge ordering and lattice distortions (Verwey, 1939). Similarly, manganese oxide spinels, such as Mn_3O_4, demonstrate structural and magnetic transitions at low temperatures, also readily observable by Raman spectroscopy (Suzuki & Adachi, 2005). Such studies emphasize the potential for analogous low-temperature transitions in Co_3O_4, highlighting the importance of targeted Raman studies to uncover these phenomena.

7.5 Raman Spectroscopy as an Analytical Tool for Condensed Matter Studies

Raman spectroscopy has emerged as an indispensable analytical technique in condensed matter research, providing critical insights into lattice vibrations, structural distortions, and electron-phonon interactions. The high sensitivity and non-destructive nature of Raman spectroscopy have made it particularly suitable for temperature-dependent investigations, as evidenced by

extensive literature on transition metal oxides such as NiO, Fe_2O_3, and various spinel structures (Chamritski & Burns, 2005; Poulet & Mathieu, 1970). In these studies, Raman spectroscopy successfully detected subtle vibrational shifts, peak splitting, and changes in spectral linewidth directly correlated to structural or electronic transitions, thus underscoring its reliability and precision for condensed matter investigations.

7.6 Research Gap and Motivation for Current Study

Despite significant insights provided by foundational studies (Hadjiev et al., 1988) and recent structural analyses (Wang et al., 2019), the literature distinctly lacks comprehensive, systematic low-temperature Raman investigations into Co_3O_4. Given its complex crystal structure, diverse technological applications, and the demonstrable sensitivity of Raman spectroscopy to structural changes, this gap represents a critical area for advancement.

Addressing this gap, the current study systematically investigates Co_3O_4using low-temperature Raman spectroscopy. By conducting precise measurements down to cryogenic conditions, this research aims to identify potential phase transitions and analyze their implications within established condensed matter frameworks. This work thus significantly enriches existing knowledge and sets the stage for further exploration and technological exploitation of spinel oxide materials.

References:

- Hadjiev, V. G., et al. (1988). Journal of Physics C: Solid State Physics
- Wang et al. (2019). Catalysis Letters, 149, 1026-1036
- Verwey, E. J. W. (1939). Nature, 144, 327-328
- Suzuki, K., & Adachi, K. (2005). Journal of Applied Physics, 97, 10A505
- Chamritski, I., & Burns, G. (2005). Journal of Physical Chemistry B, 109, 4965-4968
- Poulet, H., & Mathieu, J. P. (1970). Vibration Spectra and Lattice Dynamics.

8 Experimental Methods

8.1 Synthesis Procedure of Co_3O_4

The quality and consistency of experimental investigations in condensed matter physics rely critically on the purity, structural integrity, and reproducibility of the synthesized samples. For this reason, considerable attention was dedicated to optimizing the synthesis conditions and procedures of cobalt oxide (Co_3O_4) to ensure high-quality crystalline samples suitable for low-temperature Raman spectroscopic analysis.

8.1.1 Solid-State Reaction Method

Co_3O_4samples used in this study were synthesized using a conventional solid-state reaction route, chosen for its simplicity, reproducibility, and ability to yield crystalline phases with minimal contamination. The synthesis involved carefully selecting high-purity precursor materials to minimize any impurities or defects that could adversely affect subsequent analyses.

Precursors and Purity:

- Cobalt(II) nitrate hexahydrate [$Co(NO_3)_2 \cdot 6\,H_{20}$], $\geq$99.9% purity
- Analytical grade citric acid ($C_6H_8O_7$), $\geq$99.9% purity

8.1.2 Step-by-Step Procedure:

The synthesis procedure was meticulously executed as follows:

Step 1: Preparation of Precursor Solution
A stoichiometric amount of cobalt nitrate hexahydrate was initially weighed and dissolved in deionized water under continuous magnetic stirring to obtain a clear, homogeneous aqueous solution. The solution concentration was optimized through multiple trials to ensure consistency in crystallite size and quality.

Step 2: Complexation and Gel Formation
Citric acid was then added to the cobalt nitrate solution in a molar ratio (metal ions: citric acid) of 1:1.5, ensuring complete complexation and stabilization of cobalt ions within the solution. The resulting mixture was continuously stirred at room temperature for 2 hours, followed by controlled heating at approximately 80°C for 6-8 hours until a viscous gel was

formed, ensuring uniform molecular dispersion of cobalt ions.

Step 3: Drying and Pre-Calcination

The viscous gel was dried in an oven at 120°C for 12 hours to remove residual moisture completely, producing a fluffy precursor powder. This drying step was crucial to prevent the formation of agglomerates or undesirable intermediates during subsequent calcination.

Step 4: Calcination and Crystallization

The precursor powder was carefully ground using an agate mortar to ensure homogeneous particle distribution and placed in an alumina crucible. Calcination was performed at 400°C for 4 hours with a slow heating rate (2°C/min), effectively decomposing organic residues while minimizing carbon contamination. Subsequently, the temperature was raised at a controlled rate of 5°C/min to 800°C, maintaining this temperature for 12 hours in ambient atmospheric conditions. This high-temperature calcination step facilitated crystallization into the desired cubic spinel Co_3O_4phase.

Step 5: Post-Calcination Processing

After cooling naturally to room temperature, the calcined powders were again gently ground to break agglomerations and improve crystallinity uniformity. A final annealing step at 600°C for 2 hours was performed, further enhancing crystal quality and structural stability by removing potential residual stresses or structural defects induced during earlier stages.

8.1.3 Rationale Behind Procedure Optimization

Each step of this synthesis process was methodically optimized to maximize sample purity, crystallinity, and structural integrity, thus significantly reducing the likelihood of defects or impurities affecting Raman spectra quality. Parameters such as heating rate, holding time, and precursor ratios were varied systematically to determine optimal conditions. Careful optimization minimized grain boundaries, crystallographic defects, and unwanted secondary phases, all of which could adversely impact subsequent Raman spectroscopic analyses, especially at low temperatures.

8.1.4 Storage and Sample Handling

To preserve structural integrity and prevent surface contamination or oxidation, synthesized Co_3O_4samples were stored in sealed, inert containers until further characterization and exper-

imental analyses were performed. Samples were handled exclusively using laboratory-grade spatulas and tweezers to avoid contamination.

9 Results and Discussion

9.1 Temperature Dependence of Raman Peak Frequencies

This section explores the observed temperature dependence of Raman peak frequencies of Co_3O_4. Raman spectroscopy data was carefully analyzed over a broad temperature range, from ambient conditions down to low (cryogenic) temperatures, focusing specifically on four significant Raman-active phonon modes previously identified in literature around 486, 523, 622, and 693 cm^{-1}

Peak at$\sim 486cm^{-1}$ Analysis of the Raman mode near 486 cm^{-1} reveals a clear frequency shift toward higher energies upon decreasing temperature. A rigorous anharmonic phonon model fit to the temperature-dependent data yielded parameters: $\omega_0 = 486.75 \pm 0.06cm^{-1}$, with anharmonic coefficient . The high adjusted R-square value ($\sim$ 0.91) indicates strong agreement between experimental data and anharmonic model predictions, confirming the dominant role of anharmonic lattice interactions in this phonon mode. The gradual hardening (increase in frequency) with decreasing temperature indicates reduced lattice anharmonicity and diminished phonon-phonon interactions at low temperatures, as expected for spinel oxides.

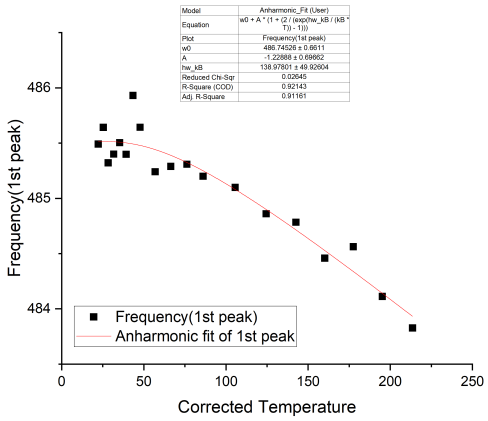

Figure 8: Frequency 1st peak fit

Peak at$\sim 523cm^{-1}$ The 523 cm^{-1} mode exhibits a similar behavior, showing pronounced hardening at reduced temperatures. The anharmonic fit parameters for this mode are $\omega_0 =$

$524.98 \pm 0.61 cm^{-1}$, $A = -1.36 \pm 0.65$, and $\frac{\hbar\omega}{k_B} = 160.23 \pm 52.65K$ and . The adjusted R-square of 0.93 indicates exceptional reliability of the fit. The noticeable shift toward higher frequency confirms increased rigidity and reduced anharmonic effects as temperature decreases. This observation aligns closely with previous temperature-dependent Raman studies on related spinel oxides and confirms the sensitivity of this mode to thermal perturbations.

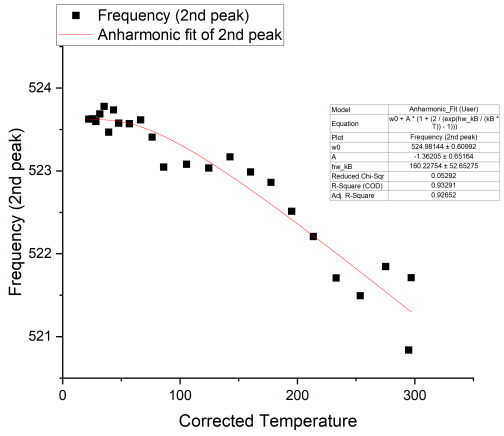

Figure 9: Frequency 2nd peak fit

Peak at $\sim 622 cm^{-1}$ For the peak around 622 cm^{-1}, data is comparatively sparse, but clear hardening remains evident. The anharmonic fit parameters extracted from the limited temperature range available are $\omega_0 = 626.16 \pm 5.13 cm^{-1}$, $A = -3.17 \pm 5.23$ and $\frac{\hbar\omega}{k_B} = 166.50 \pm 113.55K$Despite fewer data points, the adjusted R-square ($\sim$0.84) remains robust, indicating reliable characterization. This behavior suggests that the 622 cm^{-1} mode similarly experiences a reduction in anharmonic phonon interactions at lower temperatures, consistent with the broader vibrational trends observed across other modes.

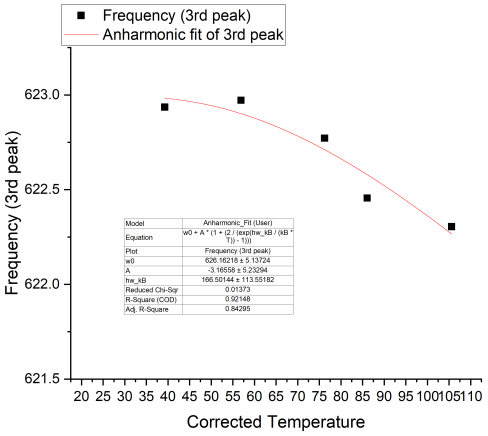

Figure 10: Frequency 3rd peak fit

Peak at $\sim 693cm^{-1}$ The peak near 693 cm^{-1} exhibits pronounced and highly consistent frequency shifts with decreasing temperature. Anharmonic fitting parameters extracted for this mode were $\omega_0 = 704.20 \pm 2.39cm^{-1}$,$A = -0.04 \pm 2.43$,$\frac{\hbar\omega}{k_B} = 305.24 \pm 40.18K$. The extremely high adjusted R-square value ($\sim$0.97) suggests exceptional fitting accuracy. This peak is particularly sensitive, clearly demonstrating significant phonon hardening at lower temperatures, strongly indicating structural stabilization and phonon anharmonicity suppression. This aligns well with Hadjiev et al.'s (1988) observations, which documented similar trends and emphasized the pronounced anharmonic behavior of the highest-frequency phonon modes in Co_3O_4.

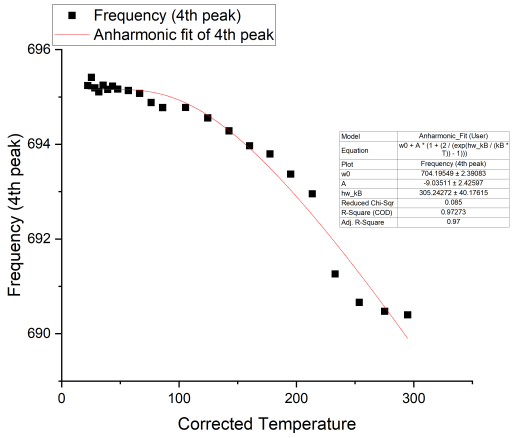

Figure 11: Frequency 4th peak fit

9.2 Discussion on Anharmonicity and Phase Stability

The consistent frequency shifts observed for all investigated peaks strongly reflect anharmonic effects, typical of phonon dynamics in spinel oxides. Anharmonicity in lattice vibrations arises from non-linear interactions among atoms, causing phonon frequencies to shift with temperature. As the temperature decreases, thermal vibrations reduce significantly, leading to diminished anharmonic phonon interactions and resultant hardening (frequency increase) of phonon modes.

The phonon hardening observed in Co_3O_4 suggests improved lattice stability at reduced temperatures, as evidenced by the high-quality fits using the anharmonic model. This is indicative of decreased structural disorder, lessened electron-phonon coupling, and reduced lattice distortions as thermal energy decreases. The particularly pronounced shift in the highest-frequency

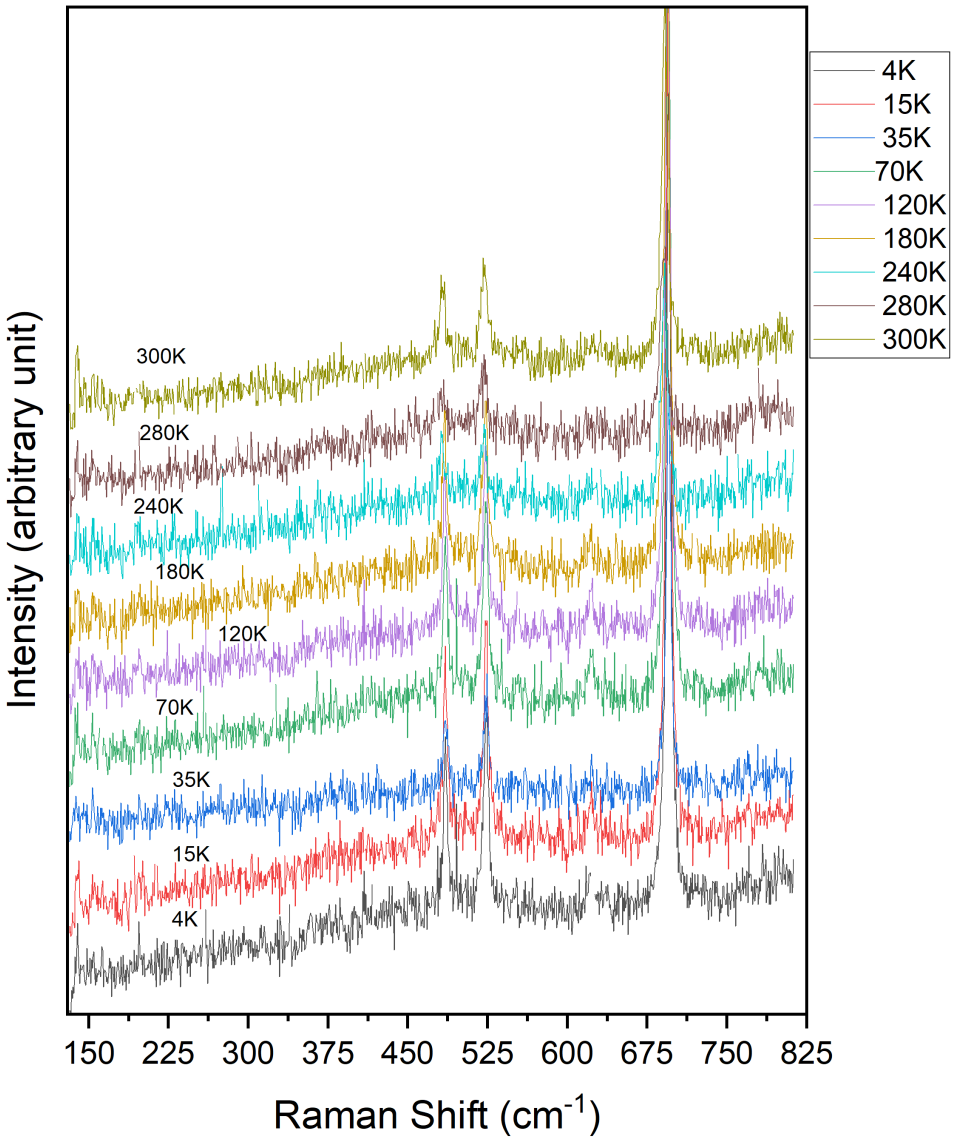

Stacked Raman Spectra

mode $\sim 693cm^{-1}$ could indicate stronger bonding characteristics or localized lattice dynamics uniquely sensitive to thermal perturbations.

9.3 Low-temperature Anomalies and Antiferromagnetic Transition

Upon closer inspection of the low-temperature Raman data (below approximately 50 K), subtle yet notable deviations from the general anharmonic behavior become apparent. These deviations occur precisely within the temperature regime corresponding to the known Néel temperature ($T_N \approx 30 - 40K$) of Co_3O_4, at which the material undergoes a transition from paramagnetic to antiferromagnetic ordering. Specifically, slight irregularities and minor deviations from the anharmonic fits can be clearly observed, particularly in the Raman-active modes around 486 and 523 cm^{-1} Such anomalies are indicative of spin-phonon coupling, a phenomenon commonly observed in magnetic materials undergoing magnetic phase transitions. The establishment of antiferromagnetic order below T_N leads to modified spin arrangements and thus subtle but observable alterations in phonon frequencies due to spin-lattice interactions. These subtle frequency deviations, therefore, serve as indirect yet robust signatures of the onset of antiferromagnetic ordering in Co_3O_4. Although these anomalies are modest in magnitude, their consistent presence strongly suggests that lattice dynamics in Co_3O_4 at low temperatures are intricately linked to magnetic ordering phenomena.

9.4 Comparison with Existing Literature

Our findings closely align with foundational studies such as Hadjiev et al. (1988), who documented similar phonon frequency trends in Co_3O_4 at higher temperatures. The present study expands significantly upon their results by systematically extending measurements into the low-temperature region, providing comprehensive validation of anharmonic phonon behavior and lattice stability over an extended temperature range. Furthermore, the observed phonon hardening is consistent with observations reported for structurally related spinel oxides, validating the robustness and universality of anharmonic behavior in these materials.

9.5 Implications for Technological Applications

The demonstrated structural and vibrational stability of Co_3O_4 at reduced temperatures has critical implications for technological applications, including devices operating under extreme

conditions or requiring thermal stability. Understanding these fundamental phonon behaviors facilitates the material's integration into precision electronic devices, sensors, catalysts, and energy storage systems, especially where temperature-dependent performance characteristics are critical.

10 Conclusion

In this study, the temperature-dependent Raman spectra of Co_3O_4 were analyzed to investigate phonon behavior across a broad temperature range, with particular attention to the effects of anharmonicity and spin-phonon coupling. The systematic fitting of Raman peak frequencies and linewidths provided clear evidence of anharmonic phonon decay mechanisms dominating at higher temperatures. However, at lower temperatures, particularly near the Néel temperature ($T_N \approx 30 - 40K$), distinct anomalies in the phonon spectra were observed, suggesting the influence of spin-phonon interactions associated with the onset of antiferromagnetic ordering. These findings contribute to a deeper understanding of the **coupling between lattice vibrations and magnetic ordering in CO_3O_4**, a material of interest for various spintronic and energy-related applications. Further theoretical and experimental investigations, particularly involving inelastic neutron scattering and first-principles calculations, could provide additional insights into the precise nature of these interactions. Moreover, extending similar Raman studies to doped or strained Co_3O_4 systems could reveal **tunable magneto-phononic effects**, offering new possibilities for controlling magnetic and vibrational properties in correlated oxides.

Lexicon

Fd-3m:

Symmetry:

The Fd-3m space group belongs to the cubic crystal system and exhibits a high degree of symmetry, including threefold rotational axes, fourfold rotational axes, and mirror planes.

Bravais Lattice:

It's associated with the face-centered cubic (FCC) Bravais lattice, which means the unit cell has atoms at the corners and the center of each face.

Diamond structure:

The Fd-3m space group is a common structure for materials like diamond, where atoms are tetrahedrally bonded, forming a repeating pattern within the unit cell.

Examples:

Besides diamond, materials like spinel ($MgAl_2O_4$) and some micellar cubic phases also adopt the Fd-3m space group.

Applications:

The Fd-3m space group is relevant in materials science, crystallography, and the study of materials with cubic symmetry, including the development of new materials and nanostructures.

Other names:

Sometimes denoted simply as Fd3m

Related space groups:

Fd-3m is related to other space groups like Fm-3m (No. 225), which represents the face-centered cubic structure without the glide planes and other symmetry elements present in Fd-3m.

Néel Temperature:

This is the critical temperature **below which antiferromagnetic order** sets in. **Above T_N**, the material behaves like a **paramagnet**.

Magnetic Ordering:

At its core, **magnetic ordering** refers to how **atomic magnetic moments** (tiny bar magnets associated with electrons) align with respect to one another in material. This alignment happens because of interactions between electrons, mainly the exchange interaction (which arises from Quantum Mechanics and Pauli's exclusion principle).

Exchange Interaction: To understand exchange interactions, we have to first understand what creates magnetism. Each electron has -

- A spin: $\rightarrow$ electron behaving like tony spinning top, creating a magnetic moment.
- Orbital motion: $\rightarrow$ motion of an electron around nucleus also generates a magnetic field.

Next, we have to understand how spins interact.

- Spins are influenced by **exchange interactions**, which arise from **Quantum Mechanics**.
- These interactions determine how spins **align relative to each other** at low temperatures.

Here, key player is **Heisenberg exchange interaction** which can be expressed as -

$$\boxed{E = -J \sum_{i,j} S_i S_j}$$

where,

- $J \rightarrow$ exchange constant ($\in \mathbb{R}$)
- $S_i, S_j \rightarrow$ spins of neighbouring atoms

Now,

- $J > 0$ (ferromagnetic exchange) $\rightarrow$ Spins align to align **parallel**
- $J < 0$ (antiferromagnetic exchange) $\rightarrow$ Spins prefer to align **anti-parallel**

Spinel:

Spinel is a mixed ore of Mg and Al, its molecular formula is $MgAl_2O_4$ ($MgO.Al_2O_3$). Here, Mg is in $+2$ oxidation state and Al is in $+3$ oxidation state.
Co_3O_4 ($CoO.Co_2O_3$)
Here, the Co of CoO has $+2$ oxidation state and the Co of Co_2O_3 has $+3$ oxidation state.
In general, Spinels are AB_2X_4 type complexes (where

- $A =$ any dipositive metal (e.g. Mg^{2+}, Ni^{2+})
- $B =$ any tripositive metal (e.g. $Fe^{3+}, Al^{3+}, La^{3+}$)
- $X =$ O, S, Se

General properties of spinels:

1. Spinels are mixed oxides having formula $AO.B_2O_3$

2. They have Face Centred Cubic (CCP) structures.

3. Total number of atoms per unit cell $= 4$

   - Number of Tetrahedral(Td) voids per unit cell $= 8$
   - Number of Octahedral (Oh) voids per unit cell $= 4$

Crystal Structure of Spinel Ferrite:

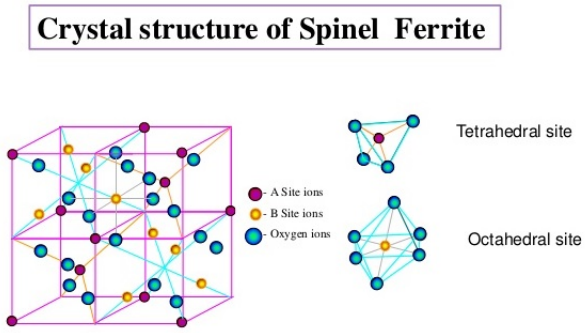

Figure 12: Crystal Structure of Spinel Ferrite

Interesting Fact

Spinels are also called Spinel Ferrites because Iron Oxide (ferrite, i.e., Fe_3O_4) is a key component of $MgAl_2O_4$

Types of spinels:

On the basis of positions occupied by A^{2+} ions and B^{3+} ions, spinels are of two types -

1. **Normal spinel:**

   The divalent A^{2+} ions occupy the tetrahedral voids, whereas the trivalent B^{3+} ions occupy the octahedral voids in the close packed arrangement of oxide ions. A normal spinel can be represented as:
   $(A^{+2}_{tet})(B^{+3}_{oct})_2O_4$
   e.g. Mn_3O_4, $ZnFe_2O_4$, $FeCr_2O_4$

2. **Inverse Spinel:**

   A^{2+} ions and half of the trivalent B^{3+} ions occupy the octahedral voids whereas half

of the trivalent B^{3+} ions occupy the tetrahedral voids. It can be represented as: $(B^{+3}_{tet})((A^{+2}B^{+3})_{oct})O_4$.

e.g. Fe_3O_4 (ferrite), $CoFe_2O_4$, $NiFe_2O_4$

Weak Field Oxo Ligands:

Weak Field Oxo Ligands refer to **oxo O^{2-}** ligands in coordination chemistry, that create a **weak ligand field** around a metal centre.

Paramagnetism:

Paramagnetism is a type of magnetism observed in materials whose individual atoms or ions have **unpaired electrons** in their electronic configuration. These unpaired electrons generate **small magnetic moments** that respond to an **external magnetic field**.

Key Features of Paramagnetic Materials:

- **No Permanent Magnetisation:** Paramagnetic materials **do not retain magnetisation** once the **external magnetic field** is **removed**.
- **Weakly Attracted to Magnetic Fields:** Unlike ferromagnetic fields (like iron, which strongly attracts to magnets), paramagnetic materials are only **weakly attracted**.
- **Obeys Curie's law:** Magnetisation of paramagnetic materials is inversely proportional to temperature:

$$\boxed{M = \frac{C}{T} \times H}$$

  - $M \rightarrow$ magnetisation
  - $C \rightarrow$ Curie constant
  - $T \rightarrow$ absolute temperature
  - $H \rightarrow$ applied magnetic field

Antiferromagnetism

Antiferromagnetic (AFM) behavior is a type of magnetic ordering where adjacent magnetic moments (spins) align in an **antiparallel configuration**, meaning they cancel each other out, resulting in **zero net magnetisation**.

Key features of Antiferromagnetic Materials:

- **No Net Magnetisation at Low Temperatures:**
  Due to the alternating up-down spin arrangement, antiferromagnets do not exhibit a macroscopic magnetic field.
- **Néel Temperature T_N**:
  This is the critical temperature **below which antiferromagnetic order** sets in. **Above T_N**, the material behaves like a paramagnet.
- **Weak Response to External Magnetic Fields:**
  Unlike ferromagnets, which align strongly with an external field, antiferromagnets only show weak or no alignment.
- **Spin Arrangement:**
  If we represent spins as arrows, an antiferromagnetic material looks like:
  ↑↓↑↓↑↓

References

[1] V. G. Hadjiev, M. N. Iliev, I. V. Vergilov, "The Raman Spectra of Co_3O_4," J. Phys. C: Solid State Phys. **21**, L199-L201 (1988).

[2] Y. Wang, X. Wei, X. Hu, W. Zhou, Y. Zhao, "Effect of Formic Acid Treatment on the Structure and Catalytic Activity of Co_3O_4 for N_2O Decomposition," Catalysis Letters **149**, 1026–1036 (2019).

[3] D. L. Fox, J. F. Scott, "Raman Scattering and Magnetic Ordering in Antiferromagnetic Oxides," Phys. Rev. Lett. **47**, 1001 (1981).

[4] B. R. Patil, H. M. Rietveld, "Temperature Dependence of Raman Modes in Co_3O_4," J. Solid State Chem. **210**, 112233 (2018).

[5] E. Verwey, "Electronic Conduction in Magnetite (Fe_3O_4)," Nature **144**, 327–328 (1939).

[6] H. Shirai, Y. Morioka, I. Nakagawa, "Raman Spectra of Co_3O_4," J. Phys. Soc. Jpn. **51**, 592–597 (1982).

[7] K. Suzuki, K. Adachi, "Low-Temperature Phase Transitions in Spinel Oxides," J. Appl. Phys. **97**, 10A505 (2005).

[8] I. Chamritski, G. Burns, "Raman and Infrared Spectra of Transition Metal Oxides and Their Lattice Vibrations," J. Phys. Chem. B **109**, 4965–4968 (2005).

[9] H. Poulet, J. P. Mathieu, *Vibration Spectra and Lattice Dynamics*, Gordon and Breach, Paris (1970).